

# Infrared and millimetre-wavelength evidence for cold accretion within a $z = 2.83$ Lyman- $\alpha$ Blob

Daniel J.B. Smith<sup>1,2\*</sup>, Matt J. Jarvis<sup>3</sup>, Mark Lacy<sup>4</sup> and Alejo Martínez-Sansigre<sup>5</sup>

<sup>1</sup>*Astrophysics Research Institute, Liverpool John Moores University, Twelve Quays House, Egerton Wharf, Birkenhead, CH41 1LD, UK*

<sup>2</sup>*Department of Astrophysics, University of Oxford, Denys Wilkinson Building, Keble Road, Oxford, OX1 3RH, UK*

<sup>3</sup>*Centre for Astrophysics, Science & Technology Research Institute, University of Hertfordshire, Hatfield, Herts, AL10 9AB, UK*

<sup>4</sup>*Spitzer Science Center, California Institute of Technology, Pasadena, CA, USA*

<sup>5</sup>*Max-Planck-Institut für Astronomie, Königstuhl 17, D-69117 Heidelberg, Germany*

25 October 2018

## ABSTRACT

This paper discusses infrared and millimetre-wavelength observations of a Lyman- $\alpha$  blob discovered by Smith & Jarvis, a candidate for ionization by the cold accretion scenario discussed in Fardal et al. and Dijkstra et al. We have observed the counterpart galaxy at infrared wavelengths in deep observations with the *Spitzer Space Telescope* using the IRAC 3.6, 4.5, 5.8 & 8.0 $\mu$ m and MIPS 24 $\mu$ m bands, as well as using the Max-Planck Millimeter Bolometer Array at a wavelength of 1.2mm with the IRAM 30 metre telescope. These observations probe the  $\gtrsim 95$ kpc Lyman- $\alpha$  halo for the presence of obscured AGN components or the presence of a violent period of star formation invoked by other models of ionisation for these mysterious objects. 24 $\mu$ m observations suggest that an obscured AGN would be insufficiently luminous to ionize the halo, and that the star formation rate within the halo may be as low as  $<140 M_{\odot}\text{yr}^{-1}$  depending on the model SED used. This is reinforced by our observations at 1.2mm using MAMBO-2, which yield an upper limit of SFR  $<550 M_{\odot}\text{yr}^{-1}$  from our non-detection to a  $3\sigma$  flux limit of 0.86 mJy beam $^{-1}$ . Finding no evidence for either AGN or extensive star formation, we conclude that this halo is ionised by a cold accretion process. We derive model SEDs for the host galaxy, and use the Bruzual & Charlot and Maraston libraries to show that the galaxy is well described by composite stellar populations of total mass  $3.42 \pm 0.13 \times 10^{11} M_{\odot}$  or  $4.35 \pm 0.16 \times 10^{11} M_{\odot}$  depending on the model SEDs used.

**Key words:** Galaxies: High-Redshift, Galaxies: Haloes

## 1 INTRODUCTION

Lyman- $\alpha$  Blobs, discovered by Steidel et al. (2000), consist of amoebic structures emitting profusely at the rest-frame wavelength of the Lyman- $\alpha$  emission line, 1216Å. Whilst these very large Lyman- $\alpha$  emitting haloes are reminiscent of the extended emission line regions observed around powerful high redshift radio galaxies (e.g. Villar-Martín et al., 2007b), they typically have less than 1% of the associated radio flux, raising the question as to what ionises the neutral Hydrogen in order to enable the emission of Lyman- $\alpha$  photons. Three of the most plausible explanations for this are:

- LABs contain hidden QSOs (e.g. Haiman & Rees 2001; Weidinger, Møller & Fynbo 2004; Weidinger et al. 2005; Barrio et al., 2008). The luminous nature of LABs with typically  $L = 10^{44}$  erg s $^{-1}$  in the Lyman- $\alpha$  emission line alone suggests that the hard spectra, and bolometric luminosity of QSOs are prime candidates to power such a galaxy’s emission.

- The Lyman- $\alpha$  emission comes from a dust-enshrouded, extreme starburst galaxy with a large scale superwind due to large numbers of luminous and short-lived OB stars (e.g. Taniguchi & Shioya 2000; Ohyama et al. 2003; Wilman et al. 2005, Matsuda et al. 2007). Observational evidence from e.g. Chapman et al. (2001) and Geach et al. (2007) associating LABs with sub-millimetre galaxies suggests that some LABs contain enshrouded starbursts forming stars at rates of  $\sim 1000 M_{\odot}\text{yr}^{-1}$ .

- We are observing the cooling radiation of a collapsing protogalaxy inside a dark matter halo’s gravitational potential (the so-called “cold accretion” model - e.g. Haiman, Spaans & Quataert, 2000, Fardal et al., 2001, Matsuda et al., 2004, Dijkstra et al. 2006a,b, Nilsson et al., 2006, Dijkstra et al., 2007, Smith & Jarvis, 2007). A cold accretion scenario invokes collisional excitation and re-radiation of accreting neutral gas to power the profuse Lyman- $\alpha$  emission extended over the halo.

The sources of ionisation residing within these galaxies (which are sometimes extended over many tens of kiloparsecs), are currently thought to be diverse. This result is due to the dis-

\* E-mail: djs@astro.livjm.ac.uk(DS)

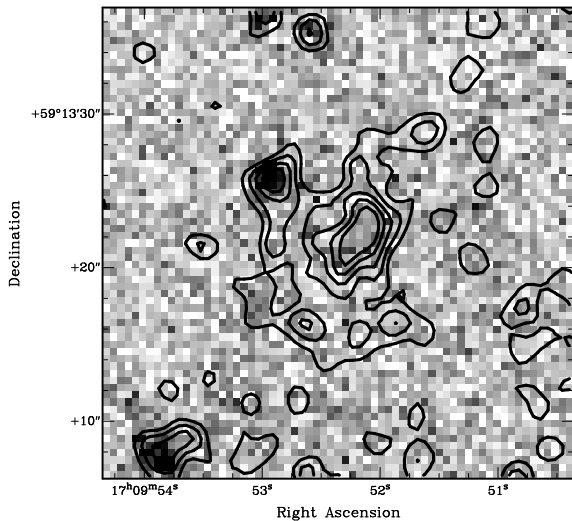


**Figure 1.** Narrow-band contour map overlaid on the Sloan-g' band data. This frame is  $\sim 33''$  on a side and North is up while East is to the left. The object to the North and East of the core of the Lyman- $\alpha$  emission is a low-redshift interloper, identified as being at  $z = 0.84$  due to the presence of [OII] $_{3727}$ , [NeIV] $_{2424}$ , MgII $_{2799}$ , and [CII] $_{2326}$  emission in our optical spectroscopy (for more details see Smith & Jarvis, 2007).

covery of a 200kpc LAB in Dey et al.(2005) associated with a  $24\mu\text{m}$  detection attributed to an obscured AGN, to the discovery by Chapman et al. (2001) of a highly luminous sub-millimetre source (with  $L_{\text{bol}} \sim 10^{13} L_{\odot}$ ) indicative of a very high star formation rate ( $\sim 1000 M_{\odot} \text{ yr}^{-1}$ ) residing within LAB1 from Steidel et al. (2000), and to the non-detection of any apparent source of ionization associated with a LAB in the GOODS-South field by Nilsson et al. (2006).

Smith & Jarvis (2007) discovered only the second known Lyman- $\alpha$  Blob thought to be ionized by the process of cold accretion, residing at  $z = 2.83$ . In figure 1 we show the Sloan-g' band image of the LAB from our survey, overlaid with a contour map of the HeII narrow-band data, sensitive to Lyman- $\alpha$  emission at the redshift of the LAB. This LAB was found to be extended over at least  $\geq 95\text{kpc}$ , with a Lyman- $\alpha$  luminosity of  $L_{Ly\alpha} = 2.1 \pm 0.5 \times 10^{43} \text{ erg s}^{-1}$ .

The LAB in question is located at  $17^{\text{h}}09^{\text{m}}52.3^{\text{s}} +59^{\circ}13'21.72''$  (J2000), on the very edge of the Extragalactic component of the *Spitzer First Look Survey* (Marleau et al., 2004, Fadda et al., 2006), and was covered with any S/N at all only in the  $4.5\mu\text{m}$  band (IRAC channel 2 - Lacy et al., 2005). In any case, the FLS observations were not deep enough for the type of study proposed here (see below).

AGN themselves are expected to be particularly dusty due to the torus invoked by schemes of AGN unification (Antonucci, 1993) to explain the different observed species; this also makes them bright at mid-infrared wavelengths since the warm torus is thought to reprocess the X-ray and UV photons emitted by the central engine. Indeed, through their mid-infrared emission, powerful AGN (quasars) can be identified up to high redshifts (e.g. Lacy et al., 2004, Martínez-Sansigre et al., 2005), even when they are so heavily obscured that they are undetected at X-ray energies (e.g. Polletta et al., 2006, Lacy et al., 2007, Martínez-Sansigre et al., 2007).

In the event that there is a  $24\mu\text{m}$  detection residing within the LAB, through studying its IR SED we would be able to distinguish between an obscured AGN and the starburst SED that would be

expected if there was extensive ongoing star formation in the LAB counterpart galaxy.

LABs ionized by a starburst are found to have very high star formation rates based on their fluxes at sub-millimetre wavelengths equivalent to  $\sim 1000 M_{\odot} \text{ yr}^{-1}$  (e.g. Chapman et al. 2001, Geach et al., 2007). The recent high-resolution Sub-Millimetre Array (SMA) observations of Matsuda et al. (2007) did not detect LAB1 from Steidel (2000), despite the bright sub-millimetre continuum measured by Chapman et al. (2001). Matsuda et al. (2007) argued that the sub-millimetre continuum was most likely resolved out by the high spatial resolution interferometric SMA observations, suggesting that the spatial extent of the sub-millimetre emitting region was  $\geq 30\text{kpc}$ , comparable to the extent of the Lyman- $\alpha$  emission itself. This reinforces the super-wind model for this LAB, in which rapid star formation within the halo is widely distributed, and could be powering the Lyman- $\alpha$  emission. Observing this new halo from Smith & Jarvis (2007) at millimetre wavelengths then provides an additional constraint on the properties of the ionizing source residing within.

Here we present the results of two independent tests for the presence of starbursting or AGN components enshrouded within the structure. This paper is organised as follows; in section 2 we describe our *Spitzer space telescope* and MAMBO-2 observations, while in section 3 we present our results, including our improved constraints on this galaxy's spectral energy distribution (SED), and section 4 presents our conclusions. Throughout this paper the AB magnitude system is used (Oke & Gunn, 1983), and a standard cosmology is assumed in which  $H_0 = 71 \text{ km s}^{-1}$ ,  $\Omega_M = 0.27$  and  $\Omega_{\Lambda} = 0.73$  (Dunkley et al., 2008).

## 2 OBSERVATIONS

### 2.1 Spitzer Space Telescope Observations

We observed the region centred on this LAB in 21 dithered 30s exposures in IRAC channels 1 & 3, and  $33 \times 30\text{s}$  in IRAC channels 2 & 4 ( $10 \frac{1}{2}$  and  $16 \frac{1}{2}$  minutes in total, respectively). We designed our  $24\mu\text{m}$  MIPS observations to use a seven-point jittering positional offset algorithm with offsets corresponding to the six nodes of a hexagon, plus the central position. We observed at each position for 501s, resulting in a total of 3507s on source. The jittering pattern was employed to ensure effective chip artefact rejection, and result in a reasonably uniform depth over the central  $5'$  of the field of view. No new MIPS channel 2 & 3 data were acquired.

These observations were carried out under program number 40957; the IRAC data in channels 1 & 3 were observed on Aug 8<sup>th</sup>, 2007, with channels 2 & 4 observed on August 12<sup>th</sup>, and the MIPS  $24\mu\text{m}$  data observed on August 22<sup>nd</sup>. The raw data were reduced, and photometric and astrometric solutions were applied automatically using the Spitzer Science Center pipeline version S16.1.0. The resulting frames are calibrated to units of surface brightness (MJy  $\text{sr}^{-1}$ ). The reduced IRAC images, centred on the LAB counterpart galaxy (circled in black) can be seen in figure 2.

The MIPS pipeline-reduced frames were reduced in seven separate parent images due to the target jitter pattern employed. They were aligned according to their astrometric solutions using the IRAF task *wregister*, before being stacked using *imcombine* (also in IRAF). The stacked MIPS data centred on the position of the LAB (again circled in black), are displayed in figure 3.

To extract meaningful fluxes from the IRAC/MIPS data, a conversion factor must be applied to convert from MJy  $\text{sr}^{-1}$  to

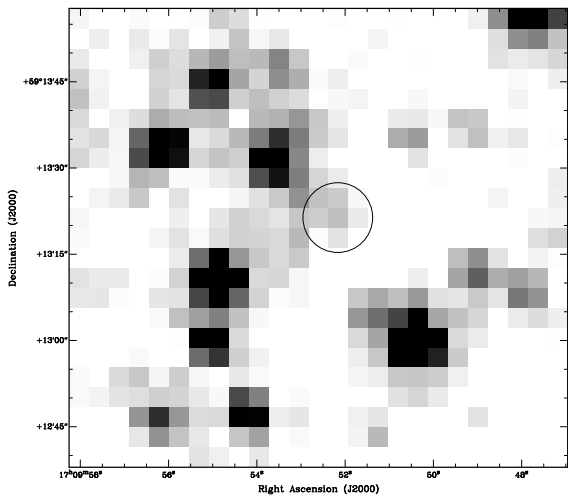


**Figure 3.** MIPS channel 1 ( $24\mu\text{m}$ ) observations centred on the LAB counterpart galaxy (circled). The galaxy is only marginally detected in this band (i.e. at  $< 3\sigma$ ); see section 3. The circle is  $12''$  in diameter.

something more useful, usually  $\mu\text{Jy pixel}^{-1}$ . The conversion factor must take into account both the difference between MJy and  $\mu\text{Jy}$ , and the difference between a steradian and the area of each pixel (see <http://ssc.spitzer.caltech.edu/fls/> for further details). Since Spitzer IRAC imaging data are calibrated to known standard source observations measured in  $10''$  apertures (for MIPS this is  $35''$ ), some correction to the photometry is necessary when measuring fluxes through apertures of different sizes due to the varying amounts of the point spread function falling within the extent of the aperture. For a  $4''$  radius aperture in IRAC this factor has values of 1.074, 1.075, 1.080 & 1.150 for channels 1 to 4 ( $3.6 - 8.0\mu\text{m}$ ), whereas for MIPS channel 1 ( $24\mu\text{m}$  band), the factor is  $\sim 2.4$ , due to the much larger PSF in MIPS data.

The MIPS  $24\mu\text{m}$  data have a  $5\sigma$  detection limit varying from  $\sim 27.4\mu\text{Jy}$  at the centre of the field of view to  $\sim 58\mu\text{Jy}$  towards the edges. We have the sensitivity to detect SFRs as low as  $200 M_{\odot} \text{ yr}^{-1}$  at  $5\sigma$  in our  $24\mu\text{m}$  data (although this does depend on the exact SED assumed, due to the relationship between  $24\mu\text{m}$  flux and far infra-red luminosity), and the accompanying IRAC sensitivity to distinguish between AGN and starbursting components, were they detected in the  $24\mu\text{m}$  band.

## 2.2 MAMBO-2 Observations

The Lyman  $\alpha$  halo was observed between 19<sup>th</sup> January and 3<sup>rd</sup> March 2008 using the Max-Planck Millimetre Bolometer Array (MAMBO-2, Kreysa et al., 1998) instrument at the IRAM 30m telescope at Pico de Veleta, Spain. The effective frequency of MAMBO-2 is 250GHz, which corresponds to 1.2mm, with a beam FWHM of  $10.7''$ . The observations were carried out in mostly clear conditions with atmospheric opacity  $\tau_{1.2 \text{ mm}} < 0.3$  and low sky noise ( $< 70 \text{ mJy beam}^{-1}$ , with most of the scans having  $\leq 40 \text{ mJy beam}^{-1}$ ). The targets were centred on the most sensitive pixel (number 20) and standard on-off observations were carried out with a wobbler throw in azimuth of  $35-45''$ , at a rate of 2 Hz to enable effective sky subtraction. Individual scans of typically 20 minutes were carried out, and the total integration time was 212 minutes.

To enable effective sky-subtraction, reduce systematic errors and avoid false positive detections, we varied the wobbler throw be-

**Table 1.** Photometric data for the LAB. Magnitudes are measured in apertures with  $4''$  radii (with the exception of the 1.2mm data, for which the beam FWHM is  $10.7''$ ), and where they are limits, they are to  $1\sigma$ . The 1.2 mm flux is calculated as detailed in the text, while the radio limits are calculated according to the local rms noise in the images. The large error in the HeII narrow-band filter has several causes; the faintness of the LAB, the difficulty in fitting the sky background due to the very extended nature of the LAB, and the presence of the nearby low- $z$  interloper to the North and East of the LAB counterpart galaxy all contribute. Some values for the longer wavelength data are given in units of Jansky ( $1 \text{ Jy} = 10^{-26} \text{ W Hz}^{-1}$ ), which is deemed more appropriate.

Photometric Band	AB Magnitude/Flux
u*	$> 26.44$
RGO U	$> 27.85$
Harris B	$23.57^{+0.23}_{-0.19}$
Sloan-g'	$23.97^{+0.70}_{-0.43}$
HeII(468.6)	$22.16^{+1.46}_{-0.60}$
Harris V	$23.97^{+0.32}_{-0.25}$
R	$23.81^{+0.20}_{-0.17}$
Sloan-i'	$24.07^{+1.19}_{-0.55}$
J	$> 19.74$
K	$21.05^{+0.20}_{-0.18}$
$3.6\mu\text{m}$	$20.71^{+0.04}_{-0.04}$
$4.5\mu\text{m}$	$20.63^{+0.05}_{-0.04}$
$5.8\mu\text{m}$	$20.85^{+0.36}_{-0.27}$
$8.0\mu\text{m}$	$20.62^{+0.24}_{-0.19}$
$24\mu\text{m}$	$18.69 \pm 7.37\mu\text{Jy}$
1.2 mm	$< 290\mu\text{Jy}$
1.4 GHz	$< 20\mu\text{Jy}$
610 MHz	$< 80\mu\text{Jy}$

tween 35, 40 and  $45''$ , and scans were conducted at different times on different days. As a result it is very unlikely for the sky observations to repeatedly fall on bright nearby sources. Prior to each scan, pointing corrections were made by observing a nearby bright source, J1638+573. The focus and opacity were checked regularly (typically every 2 hours) and the focus was generally found to be stable. Gain calibration was performed using Neptune, Uranus or Mars, and monitored regularly using very bright millimetre sources (typically  $\geq 5 \text{ Jy}$ ); the resulting absolute flux scale has an uncertainty of  $\pm 20\%$ . The data were reduced by using the MOPSIC software (Zylka 1998); with these new data we have the sensitivity to effectively distinguish between the three most plausible sources of ionization.

## 3 RESULTS

Due to the crowded nature of the field around the LAB caused by the depth of the data,  $4''$  apertures were preferred over larger options to prevent the inclusion of flux from neighbouring sources (although this was not possible for the MAMBO-2 observations, due to the  $10.7''$  FWHM of the beam). The fluxes were calculated using the function APER from the IDL Astronomy Users' Library<sup>1</sup>, which computes photometry in specified apertures and background annuli. APER accounts precisely for the different contributions of different square pixels overlapping on circular apertures, of greater importance here due to the comparatively large pixel size ( $1.2''$ ). Photometry of the LAB counterpart is presented in table 1.

<sup>1</sup> <http://idlastro.gsfc.nasa.gov/>

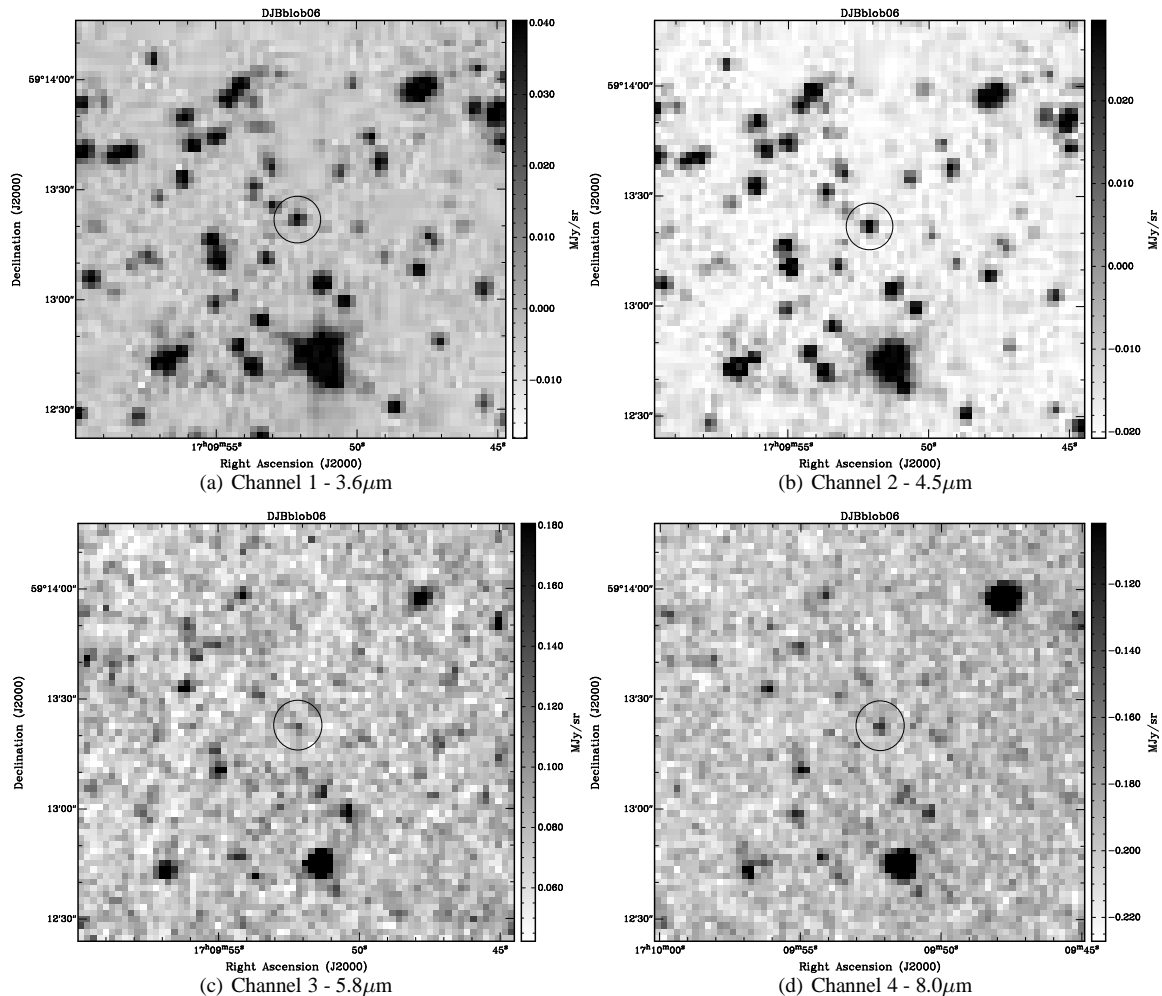


**Figure 2.** IRAC observations of the LAB counterpart galaxy. The galaxy is centred in each frame and identified by the  $12''$  diameter black circle. The counterpart galaxy is clearly detected in each band; for fluxes and errors, see table 1.

### 3.1 Searching for an obscured AGN within the LAB

To consider the possibility of an AGN residing within the halo, we examine the results of our  $24\mu\text{m}$  channel MIPS observations. Table 1 and figure 3 demonstrate the marginal detection at the position of the LAB in the MIPS  $24\mu\text{m}$  band of  $18.69 \pm 7.37 \mu\text{Jy}$  (or in AB magnitudes,  $m_{24\mu\text{m}} = 20.72^{+0.54}_{-0.36}$ ). The object is barely detected, and confusion noise is the dominant source of noise in the flux estimate. The error in this band was estimated using blank field aperture measurements of nearby regions of sky with a similar background of confusing sources. This technique was used to derive the  $24\mu\text{m}$  photometry in preference to point spread function fitting since the errors are more easily estimated (in particular, estimating the true background is almost impossible in these data due to the effects of confusion). If this marginal detection is real, it may be indicative of an obscured AGN component or an ongoing starburst residing within the halo.

To quantify the likelihood that this detection in the  $24\mu\text{m}$  band observations is real, we turn to Gaussian statistics. This value can be obtained by chance approximately 1.1% of the time given the error associated with the measurement, however this value must be treated as a lower limit due to the presence of nearby sources whose point spread functions overlap with the  $4''$  flux extraction aperture used for this measurement.

We adopt the conservative assumption that the  $24\mu\text{m}$  detection is real in order to estimate the possibility of an AGN or a starburst being the power source of the extended Lyman- $\alpha$  emission. In this way, we can estimate a limiting luminosity for any AGN residing in the LAB from the  $24\mu\text{m}$  flux density, which is not thought to be affected by dust obscuration. If this marginal detection were entirely due to an AGN, the monochromatic luminosity would correspond to a rest-frame luminosity of  $L_{\nu_{\text{RF}}} = 3 \times 10^{23} \text{ W Hz}^{-1}$  at  $\lambda_{\text{RF}} = 6.3 \mu\text{m}$ . Assuming the Elvis et al. (1994) quasar SED we estimate that this corresponds to  $L_{\text{bol}} = 3.4 \times 10^{11} L_{\odot}$  ( $1.3 \times 10^{45} \text{ erg s}^{-1}$ ), of which  $\sim 8.6 \times 10^{43} \text{ erg s}^{-1}$  is emitted at wavelengths between  $200\text{-}912\text{\AA}$  in the rest frame, and thus capable of powering Lyman- $\alpha$  emission (following Dey et al., 2005, and assuming case B recombination).

At first glance, it seems plausible that an unobscured AGN is energetically capable of powering a reasonable proportion ( $\sim 30\%$ ) of the  $2.83 \pm 0.5 \times 10^{44} \text{ erg s}^{-1}$  Lyman- $\alpha$  emission that we observe. However, we can also use a photon number counts argument similar to that in Neugebauer et al. (1980) to test the possibility of the halo being ionised by an AGN. The Lyman- $\alpha$  luminosity of the halo requires a total of  $1.7 \times 10^{55}$  ionising photons per second. Integrating under the Elvis et al. (1994) quasar SED between  $200$  and  $912\text{\AA}$  (it is only these photons which contribute to the ioni-

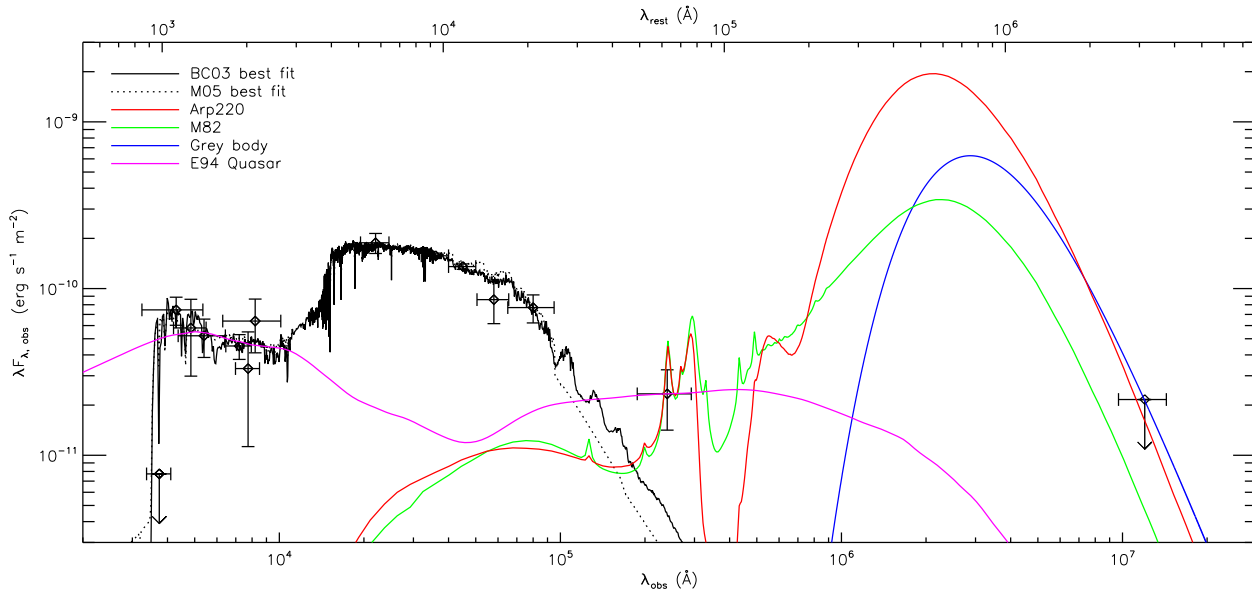


**Figure 4.** Multi-wavelength spectral energy distribution of the LAB’s counterpart galaxy. The best fit models to our photometry from the Bruzual-Charlot & Maraston simple stellar population models (solid and dotted black lines, respectively). Also included are Arp220, M82 and template QSO (from Elvis et al. 1994) SEDs shown in red, green, & purple respectively, and the best-fit grey-body emission profile (blue). The Bruzual & Charlot (2003) and Maraston (2005) SEDs are normalised to the  $3.6\mu\text{m}$  band, the Arp220, M82 and QSO templates are normalised to the  $24\mu\text{m}$  band, and the greybody is normalised to the  $1.2\text{mm}$  MAMBO-2 observations. We find that our optical & IRAC data are very well described by a composite simple stellar population consisting of a young and an old component aged 10 Myr and 0.8Gyr for the Bruzual & Charlot (2003) models, or 10 Myr and 2.0Gyr for the Maraston (2005) models. The weak detection at  $24\mu\text{m}$ , which is questionable due to its low signal-to-noise as well as the approaching confusion limit, indicates either a weak obscured AGN component or a starburst. Our other data strongly constrain these possibilities – see text. While the unobscured template quasar SED is consistent with our optical photometry, it is inconsistent with the results of our spectroscopy, which do not detect the presence of the high ionisation emission lines that the presence of such a naked AGN would suggest.

sation of neutral Hydrogen, and thus plausibly power the Lyman- $\alpha$  emission) suggests that any putative quasar component may emit only  $2.3 \times 10^{54}$  photons each second. This figure is almost an order of magnitude fewer than that required to result in the Lyman- $\alpha$  luminosity that we observe. It seems improbable that an AGN is powering the LAB; the quasar SED normalised to our  $24\mu\text{m}$  detection is displayed in figure 4.

Furthermore, it should be noted that LABs containing AGN (e.g. that which was presented in Dey et al. 2005) and the similarly luminous Lyman- $\alpha$  haloes belonging to some high redshift radio galaxies at  $z > 2$  (e.g. Villar-Martin 2007a, compared with  $24\mu\text{m}$  data from Seymour et al. 2007) are detected at mid-infrared wavelengths at fluxes typically at least an order of magnitude more luminous than those probed by our  $24\mu\text{m}$  observations. Our view that an AGN is not responsible for the Lyman- $\alpha$  emission observed here is further supported by the lack of other evidence for an AGN at radio wavelengths in the GMRT and VLA data (at 610 MHz and 1.4GHz respectively), or in our optical spectroscopy, where no other emission lines were detected (see Smith & Jarvis, 2007).

### 3.2 Constraining the star formation rate with MAMBO-2 and MIPS

To probe for evidence of the obscured star formation rates implied by superwind models of LABs of order  $\sim 1000 M_{\odot} \text{ yr}^{-1}$  (e.g. Taniguchi & Shioya, 2000), we turn first to the results of our MAMBO-2 observations. The host galaxy is not detected at  $1.2 \text{ mm}$  down to a  $3\sigma$  flux limit of  $0.86 \text{ mJy}$ . To constrain the star-formation rate probed due to cold dust masses within this halo, we consider the  $1.2\text{mm}$  (observed frame) flux to be due to a *grey body*, with

emissivity of the form given in equation 1 which is also displayed in figure 4;

$$F_{\lambda} \propto \frac{1}{\lambda} \frac{\frac{1}{\lambda}^{(4+\beta)}}{e^{\left(\frac{hc}{\lambda kT}\right)} - 1}, \quad (1)$$

where  $\beta$  corresponds to the emissivity index of the grey body spectrum and  $T$  to the temperature of the dust. We assume typical values for these two parameters from Omont et al. (2003) of  $\beta = 1.5$  and  $T=45\text{K}$ , and adopt a conversion from far-infrared luminosity between  $8 \text{ \& } 1000\mu\text{m}$  and star formation rate (SFR) following Kennicutt et al. (1998). With these assumptions we find that our  $3\sigma$  flux limit at  $1.2\text{mm}$  suggests that the star formation rate within the LAB is  $< 550 M_{\odot} \text{ yr}^{-1}$ . This puts our three sigma upper limit for the star formation rate within this LAB slightly below the SFRs required by superwind models of LAB ionization. If we adopt a slightly lower temperature for the dust component,  $T=35\text{K}$ , our estimate for the SFR within the halo becomes  $< 220 M_{\odot} \text{ yr}^{-1}$  to  $3\sigma$ .

We can also use our MIPS observations to constrain the SFR. To obtain SFR estimates from  $24\mu\text{m}$  fluxes, one must assume a particular SED in order to enable an estimate of the far infra-red luminosity, and then proceed as for the *grey-body* models. Instead of assuming a *grey-body* SED, here we use templates for M82 and Arp220 from Siebenmorgen & Krügel (2007) to derive SFR estimates. If our detection at  $24\mu\text{m}$  is real, then it corresponds to SFRs of  $\sim 140$  (M82 template) or  $620$  (Arp220 template)  $M_{\odot} \text{ yr}^{-1}$ . Given the uncertainties in these estimates, both values are consistent with the limit derived from our MAMBO-2 observations.

### 3.3 The Stellar Population

Having essentially ruled out the presence of a powerful AGN, we turn our attention to the stellar population of the LAB. The new IRAC photometry of the LAB counterpart galaxy provides much better constraints for its stellar SED, enabling us to calculate a much more effectively constrained best-fit SED, which is displayed in figure 4. The better constraints on the SED morphology then enable more accurate estimates of the stellar mass of the counterpart galaxy.

In Smith & Jarvis (2007), uncertainties in the data meant that the choice of template SEDs used for the SED fitting was not crucial; using either the Maraston (2005) or Bruzual & Charlot (2003) template SEDs made little difference to the outcome. This is no longer the case due to our new infrared and millimetre-wavelength data, combined with deeper optical data obtained from the William Herschel Telescope’s prime focus imager (PFIP) to investigate the environment of the LAB (Smith & Jarvis *in prep*). The difference between the two models (caused by different treatments of thermally pulsing asymptotic giant branch – TP-AGB – stars) at rest-frame near-infrared wavelengths becomes important due to the quality of our IRAC observations. The Maraston models are generally redder, and the effects of the TP-AGP manifest themselves as increased flux at near infrared wavelengths (e.g. Maraston, 2005). Since the models vary, we used both sets to approximate our SED. In order to enable reasonable comparisons between the best-fit models of each type, we required that both fits made use of the Salpeter (1955) initial mass functions.

The best fit SED was calculated for both species of SSP models with ages less than the 3 Gyr (the age of the Universe at  $z = 2.83$  in our adopted cosmology is 2.344 Gyr – the reason for this range of SSP ages will become clear), using a simple  $\chi^2$  fitting algorithm. We normalised the composite SED to the IRAC  $3.6\mu\text{m}$  data point (channel 1), since it has the smallest photometric errors of all bands, and is less susceptible to the effects of dust than observations in any of the shorter-wavelength bands. A variety of composite stellar SEDs were fit to our LAB counterpart photometry (table 1), consisting of linear combinations of young ( $< 600\text{Myr}$ ) and old ( $> 600\text{Myr}$ ) simple stellar populations. The best fit models based on the Bruzual-Charlot and Maraston SSPs are displayed in figure 4.

Whilst the properties of the two fits appear similar, the underlying properties are significantly different. The best-fit Bruzual & Charlot (2003) composite fit consists of a linear combination of components aged 10 Myr and 0.8 Gyr, with Salpeter IMFs (Salpeter, 1955) and solar metallicity. The best fit Maraston (2005) model comprises components aged 10 Myr & 2.0Gyr with Salpeter IMFs, and low metallicity ( $Z = 0.0001 = 1/50 Z_\odot$ ). The two best-fit models differ widely in their properties in all but the broadest sense (that the best fit consists of a composite simple stellar population with both young and old components).

Whilst the metallicities appear widely different, the discrepancy in values of  $\chi^2$  parameter suggests that our data are not capable of effectively distinguishing between different values of  $Z$ . Whilst the best-fit Maraston (2005) model has  $Z = 0.0001$  and  $\chi^2 = 10.16$ , if we set  $Z = 0.02 = Z_\odot$  then the best-fit model has  $\chi^2 = 13.19$  (albeit with a different combination of SSPs – 10 Myr & 3.0 Gyr, older than the age of the Universe at  $z = 2.83$ ). With the data available to us, attempts to effectively constrain values of the host galaxy’s metallicity are uncertain.

The masses of each component were derived from the normalisations of the models used in the  $\chi^2$  fitting process. The mass of the

**Table 2.** Properties of the best fit composite simple stellar populations for both the Bruzual & Charlot (2003) and Maraston (2005) models. The age, masses and errors are presented for both of the simple stellar populations that best fit our extensive photometry.

Parameter	Bruzual & Charlot (2003)	Maraston (2005)
Age <sub>1</sub> (Myr)	10	10
Mass <sub>1</sub> ( $M_\odot$ )	$9.06 \pm 0.34 \times 10^8$	$5.88 \pm 0.22 \times 10^8$
Age <sub>2</sub> (Gyr)	0.8	2.0
Mass <sub>2</sub> ( $M_\odot$ )	$3.41 \pm 0.13 \times 10^{11}$	$4.35 \pm 0.16 \times 10^{11}$
Mass <sub>total</sub> ( $M_\odot$ )	$3.42 \pm 0.13 \times 10^{11}$	$4.36 \pm 0.16 \times 10^{11}$
Best $\chi^2$	7.24	10.16

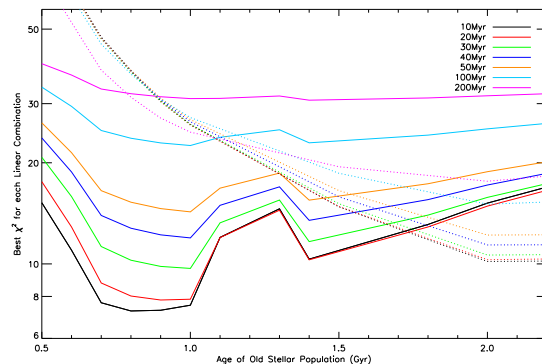


**Figure 5.** The distribution of best-fit values of  $\chi^2$  for composite Bruzual & Charlot (2003) and Maraston (2005) simple stellar populations (solid and dotted lines, respectively). The age of the best-fit old SSP component is shown on the abscissa, with the age of the best-fit young SSP component represented by the colours (see legend).

Bruzual & Charlot (2003) best-fit model is  $3.42 \pm 0.13 \times 10^{11} M_\odot$ , while for the Maraston (2005) models the total mass is  $4.36 \pm 0.16 \times 10^{11} M_\odot$ . Here, the errors are derived from the normalisation based upon the IRAC  $3.6\mu\text{m}$  flux, and are probably underestimates as a result. The details of each best-fit population, including masses, ages and errors are shown in table 2.

Since the old SSP in the Maraston model fitting scheme is older (2 Gyr) than the old SSP used in the best fit in the Bruzual-Charlot scheme, one would expect it to be more quiescent. That being the case, a larger stellar mass would be required to produce the same luminosity due to the death of the more luminous (and *shorter-lived*) stars. The different mass estimates from the Bruzual & Charlot (2003) and Maraston (2005) schemes are not unexpected, since one of the main disagreements between these two models of SEDs relates to the stellar masses implied (e.g. Maraston, 2005).

The variation of best-fit  $\chi^2$  as a function of input models is displayed in figure 5 for the two fitting regimes. A clear minimum occurs for the combination of 10 Myr & 0.8 Gyr Bruzual & Charlot templates. The preference for this model over other similar combinations is small, but this combination is the best fit, in agreement with the results of Smith & Jarvis (2007), which suggested that the counterpart galaxy was best described by a combination of a young and an old simple stellar population. The Bruzual & Charlot models (2003 - solid lines) better approximate our data than those of Maraston (2005 - dotted lines), reflected by the lower values of  $\chi^2$ .

Maraston models older than the age of the Universe are included in this analysis due to the coarse sampling of population ages above 1.5 Gyr, to enable the models to demonstrate a minimum  $\chi^2$  value. Thus we conclude that the host galaxy is well-described by a composite simple stellar population, with little or no evidence for additional (e.g. AGN) components. We also note that the composite stellar population is considerably (i.e. orders of magnitude) less luminous between 200 & 912Å than the Elvis (1994) AGN SED, and therefore also incapable of powering the Lyman- $\alpha$  halo.

#### 4 CONCLUSIONS

With our new IRAC, MIPS and MAMBO-2 data, as well as our new deep U, B & V band observations, we have demonstrated that the counterpart galaxy associated with the newly-discovered LAB announced in Smith & Jarvis (2007) is well-described by a composite stellar population. Using this new multi-wavelength data-set, we find no plausible evidence for the presence either of an obscured active galactic nucleus or of an energetic starburst that would be required to ionize the neutral Hydrogen gas in galaxy-wide superwind schemes. The most likely source of ionization for this particular highly luminous Lyman- $\alpha$  halo is a “cold accretion” scenario, which may be able to supply sufficient energy for this profuse emission without invoking either of the other power sources suggested in the literature (see Fardal et al. 2001, Dijkstra, et al., 2006a,b, 2007). We also place further constraints on the host galaxy, and find it to be well described by composite simple stellar populations with total masses of  $3.42 \pm 0.13 \times 10^{10}$  or  $4.36 \pm 0.16 \times 10^{11} M_{\odot}$ , depending on the models used.

#### ACKNOWLEDGMENTS

DJBS wishes to thank Chris Simpson for valuable conversations, and the UK STFC for a PDRA. MJJ acknowledges the support of a Research Council UK fellowship. This work is based in part on observations made with the *Spitzer Space Telescope*, which is operated by the Jet Propulsion Laboratory, California Institute of Technology under a contract with NASA. Support for this work was provided by NASA. Many thanks to the IRAM staff for their support, particularly Stéphane Leon for running the MAMBO pool, and to all guest observers during the pool observing sessions at the 30m. IRAM is supported by INSU/CNRS (France), MPG (Germany), and IGN (Spain). The Isaac Newton and William Herschel Telescopes are operated on the island of La Palma by the Isaac Newton Group in the Spanish Observatorio del Roque de los Muchachos of the Instituto de Astrofísica de Canarias.

#### REFERENCES

Antonucci R., 1993, ARA&A, **31**, 473A  
 Barrio E., et al., 2008 *submitted*  
 Bruzual G., & Charlot S., 2003, MNRAS, **344**, 1000B  
 Chapman S.C., Richards E.A., Lewis G.F., Wilson G., & Barger A.J., 2001, ApJ, **548**, L17  
 Dijkstra M., Haiman Z., & Spaans M., 2006, ApJ, **649**, 14D  
 Dijkstra M., Haiman Z., & Spaans M., 2006, ApJ, **649**, 37D  
 Dijkstra M., & Wyithe J.S.B., 2006, **375**, 1575  
 Dijkstra M., 2007, arXiv/0711.2698  
 Dunkley J., et al., 2008, arXiv-0803.0586

Efstathiou G., Rowan-Robinson M., & Siebenmorgen R., 2000, MN, **313**, 734  
 Elvis, M., et al.1994, ApJS, **95**, 1  
 Fadda et al., 2006, AJ, **131**, 2859  
 Fardal M.A., Katz N., Gardner J.P., Hernquist, L., Weinberg D.H., & Romeel D., 2001, ApJ, **562**, 605  
 Geach J.E., Smail I., Chapman S.C., Alexander D.M., Blain A.W., Stott J.P., Ivison R.J., 2007, ApJ, **655L**, 9  
 Haiman Z., Spaans M. & Quataert E., 2000, ApJ, **537**, L5  
 Haiman Z., & Rees M.J., 2001, ApJ, **553**, 545H  
 Kennicutt R.C., 1998, ARA&A, **36**, 189K  
 Kreysa E., et al., 1998, SPIE, **3357**, 319  
 Lacy, M. et al.2004, ApJS, **154**, 166  
 Lacy M., et al., 2005, ApJS, **161**, 41  
 Lacy, M., et al., 2007, AJ, **133**, 186  
 Marleau F., et al., 2004, ApJS **154** 66  
 Maraston C., 2005, MNRAS, **362**, 799M  
 Martínez-Sansigre A., Rawlings S., Lacy M., Fadda D., Marleau F.R., Simpson C., Willott C.J., & Jarvis M.J., 2005, Nature, **436**, 666  
 Martínez-Sansigre, A., et al., 2007, MNRAS, **6**, 379L  
 Matsuda Y., et al., 2004, ApJ, **128**, 569  
 Matsuda Y., Iono D., Ohta K., Yamada T., Kawabe R., Hayashino T., Peck A.B., & Petitpas G.R., 2007, ApJ, **667**, 667M  
 Neugebauer G., et al., 1980, ApJ, **238**, 502  
 Nilsson K.K., Fynbo J.P.U., Møller P., Sommer-Larsen J., Ledoux C., 2006, A&A, **452**, 23N  
 Ohyama Y., et al., 2003, ApJ, **591**, 90  
 Oke, J.B. & Gunn J.E., 1983, ApJ, **266**, 7130  
 Omont A., Beelen A., Bertoldi F., Cox P., Carilli C.L., Priddey R.S., McMahon R.G., Isaak K.G., 2003, A&A, **398**, 857  
 Pei, Y.C., 1992, ApJ, **395**, 130  
 Polletta, M., et al., 2006, ApJ, **642**, 673  
 Salpeter E.E., 1955, ApJ, **121**, 161S  
 Seymour N., et al., 2007, ApJS, **171**, 353  
 Siebenmorgen R., Freudling W., Kruegel E., and Haas M., 2004, AA, **421**, 129  
 Siebenmorgen R., & Krügel E., 2007, A&A, 461, 445S  
 Smith D.J.B., & Jarvis M.J., 2007, MNRAS, **378L**, 49S  
 Steidel C.C., Adelberger K.L., Shapley A.E., Pettini M., Dickinson M., Giavalisco M., 2000, ApJ, **532**, 170  
 Taniguchi Y. & Shioya Y., 2000, ApJ, **532**, L13  
 Villar-Martín, M., 2007, NewAR, **51**, 194V  
 Villar-Martín, M., Tadhunter, C., Morganti, R., & Holt J., 2005, MNRAS, **359**, 5  
 Weidinger M., Møller P., Fynbo J.P.U., 2004, Nature **430** 999W  
 Weidinger M., Møller P., Fynbo J.P.U., Thomsen B., 2005, A&A, **436** 825W  
 Wilman R.J., Gersten J., Bower R.G., Morris S.L., Bacon R., de Zeeuw P.T., Davies R.L., 2005, Nature, **436**, 227  
 Zylka, R. 1998, MOPSI Users Manual, (IRAM: Grenoble)

This paper has been typeset from a  $\text{\TeX}/\text{\LaTeX}$  file prepared by the author.